Manipulation of Majorana zero modes in double quantum dots

Jesus D. Cifuentes[1] and Luis G. G. V. Dias da Silva[1]

[1] *Instituto de Física, Universidade de São Paulo, C.P. 66318, 05315–970 São Paulo, SP, Brazil*

(Dated: February 11, 2019)

Luis *We'll call them Majorana "zero modes" instead of "Majorana fermions", which relates more to elementary particles.* Jesus *Ok ;)*

Majorana zero modes (MZMs) appearing at the edges of topological superconducting wires are a promising platform for fault-tolerant quantum computation. Novel proposals use MZMs tunneling inside quantum dots (QDs) to implement quantum architectures because today's precise experimental control over the QD parameters offers the unique possibility of manipulating the Majoranas inside multi-dot systems. The simplest case where Majorana manipulation is possible is in a double quantum dot (DQD). So far, no complete analysis of this basic structure has been done. This project fills this gap with an analytical and numerical quantum transport study of the effects of coupling a Majorana mode with a DQD in the non-interacting and interacting regimes. By tuning the model parameters we show that it is possible to control the the Majorana signature inside the DQD.

I. INTRODUCTION

→ *Majorana zero modes in condensed matter systems: they have been found, several papers have been written about it and there has been much progress in distinguishing them from other sources of zero-bias peaks.*

The pursuit of Majorana quasi-particles in topological superconductors has attracted significant attention in the last decades.[1,2] Since the first Kitaev's toy models[3,4] claiming promising applications to quantum computing, the field evolved rapidly towards physical realizations of the Kitaev chain. The last few decades have been full of excitement as new technological innovations allowed to document several times the observation of Majorana signatures.[5–10] One of the most promising structures is the so-called Majorana wire, which recipe consists in growing semiconducting wires with strong-orbit-coupling over proximity-induced topological (p-wave) superconductors.

These signatures are characterized by the emergence of robust zero modes localized at the edges of the material. However the observed Majorana zero-modes (MZM) have been found in superposition with other similir types of phenomenon such as the Kondo effect.[11] The new experimental proposals foucus on distinguishing MZMs from other effects and performing braiding protocols,[12–14] a basic operation for topological quantum computing.

→ *MZMs in quantum dots can co-exist with Kondo peaks.*

One of the most promising methods to detect MZMs consists in attaching a quantum dot (QD) to the edges of a Majorana chain in the topological phase and executing transport measurements through the QD.[15] In such arrangement the MZM at the end of the chain leaks inside the ,QD[16] which produces a zero-bias conductance peak of half a quanta $\frac{e^2}{2h}$ through the dot. Recently, experiments including hybrid Majorana-QD systems have been performed.[9] This method offers several advantages: 1) The qubit information is not completely destroyed, in contrast to other detection methods such as tunneling spectroscopy. 2) If performed under the Kondo temperature T_k it allows the possibility of observing the co-existance of Kondo-Majorana peaks.[17,18] 3) Today's precise experimental control over the QD parameters offers the unique possibility of manipulating MZMs inside multi-dot systems. Hence bringing new lights into the design of quantum architectures.[19,20]

Luis *Ok. Ref. 20 is PRB of scalable designs: PRB* ***95*** *235305 (2017).*

The simplest case where Majorana manipulation is possible is in a double quantum dot (DQD). However no complete analysis of the transitions of the Majorana signatures has been performed. In this paper we fill this gap by performing a detailed analysis to the model of a DQD coupled to an MZM and a metallic lead. We study the non-interancting (ballistic transport) and interacting (Numerical Renormalization Group).

→ *Here's what we did: quantum tunneling of a MZM into a double dot shows several possibilities for manipulation of MZM*

Luis *In this paper, we ...* In this paper we considered both interacting and non-interacting cases. For interacting systems we used a obtained the exact transport description . On non-interacting models we used a NRG approach. We found that in symmetric couplings In the non-interacting case, we confirmed that shifting the QD's gate voltage induces the Majorana to tunnel only to the other dot. In addition, an indirect coupling of the second dot could cause destructive interference with the Majorana signature. In the interacting case, the NRG simulations confirmed these results and showed that other interacting effects - Kondo effect and RKKY interactions[21–23] - could coexist with the Majorana signatures. On the other hand, when only one QD is coupled to the leads and the other Dot is attached to the QD, the Kondo effect is annihilated due to the destructive interference generated by extra dot.[24] Our study includes how the Majorana mode interacts with these two effects.

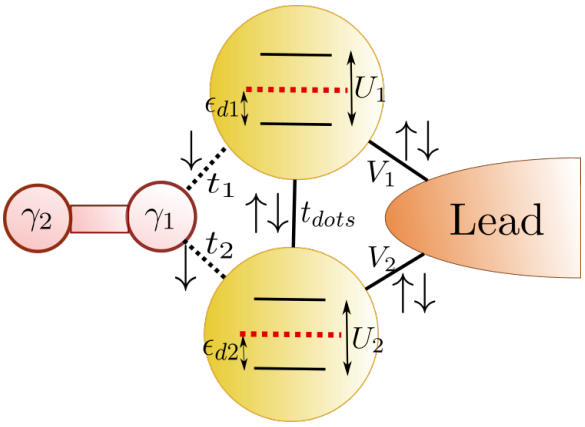

FIG. 1: DQD-Majorana set-up. Solid lines: standard coupling. Dashed lines: Majorana spin-↓ effective couplings (6). The atomic energy levels appear inside each QD. Red dashed horizontal lines represent the Fermi level.

II. MODEL AND METHODS

We consider the setup shown in Figure 1 in which a Majorana mode at the edge of Topological Superconductor(TS) is coupled to a double quantum dot (DQD), which is attached to a single metallic lead. The Hamiltonian of this system can be partitioned in four terms: the DQD Hamiltonian H_{DQD} , the Lead Hamiltonian H_{Lead} , the DQD-lead interaction $H_{DQD-Lead}$ and the coupling between the DQD and the Majorana mode H_{M-DQDs} and

$$H = H_{DQD} + H_{Lead} + H_{DQD-Lead} + H_{M-DQD} \quad (1)$$

The interacting Anderson Model describes the DQD-lead system

$$H_{DQD} = \sum_{i\in\{1,2\}} \sum_{\sigma\in\{\downarrow,\uparrow\}} \left(\epsilon_{di} + \frac{U_i}{2}\right)\hat{n}_{i\sigma} + \frac{U_i}{2}(\sum_{\sigma}\hat{n}_{i\sigma} - 1)^2 + \sum_{\sigma\in\{\uparrow,\downarrow\}} t_{dots}(d^\dagger_{1\sigma}d_{2\sigma} + d^\dagger_{2\sigma}d_{1\sigma}), \quad (2)$$

and

$$H_{Lead} = \sum_{\mathbf{k}\sigma} \epsilon_{\mathbf{k}} c^\dagger_{\mathbf{k}\sigma} c_{\mathbf{k}\sigma} \quad (3)$$

$$H_{DQD-Lead} = \sum_{\mathbf{k}\sigma} \sum_{i\in\{1,2\}} V_{i\mathbf{k}} c^\dagger_{\mathbf{k}\sigma} d_{i\sigma} + V^*_{i\mathbf{k}} d^\dagger_{i\sigma} c_{\mathbf{k}\sigma}, \quad (4)$$

where ϵ_{di} is the energy level of dot i, U_i is the Coulomb repulsion and t_{dots} is the coupling parameter between both QDs. The operator $d^\dagger_{i\sigma}$ creates a particle in dot i with spin σ and $\hat{n}_{i\sigma} := d^\dagger_{i\sigma}d_{i\sigma}$ is the particle number operator of state i. $c^\dagger_{\mathbf{k}\sigma}$ is the creation operator a particle with momentum $\mathbf{k}$ and spin σ in the lead. $\epsilon_{\mathbf{k}l}$ is the corresponding energy and $V_i(\mathbf{k})$ describes the tunneling coupling between the lead and dot i .

The Majorana modes are modeled as a superposition of the creation and annihilation operators of a spin ↓ particle $f_\downarrow$

$$\gamma_1 := \frac{1}{\sqrt{2}}\left(f^\dagger_\downarrow + f_\downarrow\right), \gamma_2 := \frac{i}{\sqrt{2}}\left(f^\dagger_\downarrow - f_\downarrow\right). \quad (5)$$

This makes possible to define an effective coupling between the Majorana Mode and the DQD by attaching γ_1 with the spin-↓ channel in the QDs

$$H_{M-DQD} = \sum_{i=1}^{2} t_i\left(d^\dagger_{i\downarrow}\gamma_1 + \gamma_1 d_{i\downarrow}\right) + \epsilon_M\gamma_1\gamma_2. \quad (6)$$

where t_i is the coupling parameter between the Majorana mode and QD i. ϵ_m is the coupling energy between both Majorana modes.

A. Methods

B. Non-interacting system

Using Zubarev's ballistic transport approach[25], we derived an exact expression for the Green functions associated to both quantum dot operators $(G_{d_1 d_1^\dagger}(\omega), G_{d_2 d_2^\dagger}(\omega))$. The detailed procedure is included in Appendix A. The transport equations define a 9×9 linear system where the Hamiltonian parameters $(t_1, t_2, \epsilon_1 \ldots)$ and the energy ω are taken as algebraic variables. The solution of this type of equations is a polynomial fraction of the same degree which makes difficult to provide an exact solution using analytical or numerical methods. To bypass this problem, we associated this transport system to a flow graph and executed a Graph-Gauss-Jordan elimination process[26]. This method proofed to be efficient to solve complex transport systems since the graph structure allows us to identify minimum cutting points and create an algorithmic representation of the Green function.

At the end, we obtained the following analytical expression

$$G_{d_{1\downarrow},d^\dagger_{1\downarrow}}(\omega) = \frac{1}{\omega - \epsilon^+_{DQD} - \frac{\|T_+\|^2}{\omega-\epsilon_{M2}-\frac{\|T_-\|^2}{\epsilon^-_{DQD}}}}. \quad (7)$$

Where

$$\epsilon^\pm_{DQD} = \pm\epsilon_1 + \sum_{\mathbf{k}}\frac{V_1V_1^*}{\omega-\epsilon_{\mathbf{k}}} + \frac{\left\|\pm t_{dots} + \sum_{\mathbf{k}}\frac{V_1V_2^*}{\omega-\epsilon_{\mathbf{k}}}\right\|^2}{\omega\pm\epsilon_2 - \sum_{\mathbf{k}}\frac{V_2V_2^*}{\omega-\epsilon_{\mathbf{k}}}}, \quad (8)$$

$$T_{\pm} = \pm t_1 \pm t_2 \frac{\left(\pm t_{dots} + \sum_{\mathbf{k}} \frac{V_1 V_2^*}{\omega - \epsilon_{\mathbf{k}}}\right)}{\omega \pm \epsilon_2 \pm \sum_{\mathbf{k}} \frac{V_2 V_2^*}{\omega - \epsilon_{\mathbf{k}}}}, \tag{9}$$

and

$$\epsilon_{M2} = \omega - \epsilon_M - \frac{\frac{\omega}{\omega+\epsilon_M} \|t_2\|^2}{\omega - \epsilon_2 - \sum_{\mathbf{k}} \frac{V_2 V_2^*}{\omega - \epsilon_{\mathbf{k}}}} - \frac{\frac{\omega}{\omega+\epsilon_M} \|t_2\|^2}{\omega + \epsilon_2 - \sum_{\mathbf{k}} \frac{V_2 V_2^*}{\omega + \epsilon_{\mathbf{k}}}}. \tag{10}$$

On the other hand the spin-↑ DOS, which is not coupled to the MZM, can be obtained by taking $t_1, t_2 = 0$, hence giving

$$G_{d_{1\uparrow}, d_{1\uparrow}^\dagger}(\omega) = \frac{1}{\omega - \epsilon_{DQD}^+}. \tag{11}$$

The final results will depend on the broadening parameter of QD i with the lead (Γ_i). This broadening satisfies the equation

$$-i\Gamma_i = \lim_{s \to 0} \sum_{\boldsymbol{k}} \frac{V_i^* V_i}{\omega + is - \epsilon_{\boldsymbol{k}}}. \tag{12}$$

By convention we take Γ_1 as the energy unit for the rest of the project. Finally we compute the DOS

$$\rho_{1\sigma}(\omega) = -\frac{1}{\pi} \mathrm{Im}\left[G_{d_{1\sigma}, d_{1\sigma}^\dagger}(\omega))\right]. \tag{13}$$

Similar results can be obtain for the DOS of the second $\rho_{2\sigma}$ by exchanging the indexes 1 and 2 in equation (11).

The density of states provides significant information about the presence of a Majorana zero modes in the dot. We characterize the Majorana signature by a robust zero-mode with two possible heights:

- **Type I:** The spin-↓ DOS is the half of the spin-↑ DOS at the Fermi energy ($\rho_\downarrow(0) = \rho_\uparrow(0)$).
- **Type II:** A spin-↓ zero mode of height $\rho_\downarrow(0) = \frac{0.5}{\pi\Gamma_1}$.

In our results we observe several times these two types of signatures. Type I often appears when there is a zero-mode in the spin-↑ DOS. Type II emerges in the other situations.

C. Interacting case (NRG)

The Numerical Renormalization Group (NRG)[27–29] is the most successful methods to study interacting quantum impurity models. In this project, the impurity is described by the DQD attached to a Majorana mode. Our code a coulomb repulsion factor of $U = 17.3\Gamma_1$ in both dots and a cut-off energy of $D = 2U = 34.6\Gamma_1$. The spacing with other energy levels is assumed to be higher than D, such that only the two coulomb states are relevant for the system dynamics. Particle-Hole-Symmetry at each dot is obtained when $\epsilon_i = \frac{U}{2}$ in both dots. At this point, each dot has an odd number of electrons, hence, at sufficiently low temperature the system will exhibit the characteristic Kondo peaks at the Fermi energy Wilson[27]. The coexistence of Kondo and Majorana zero modes is still a point of contention in the area and one of the objectives of this part of the project

To improve the efficiency of the code we used the symmetries of the system to maintain a block structure during NRG's iterative diagonalization process. This model preserves the spin-↑ particle number $\hat{N}_\uparrow$ and the spin-↓ parity $\hat{P}_\downarrow = \pm$ (+ even, − odd). The spin-↓ particle number is not preserved due to superconducting-type Majorana coupling (6) . The initial Hamiltonian is organized in blocks according to these symmetries. This block structure is preserved during the entire iteration process[29]. To compute the spectral functions, we use the density matrix renormalization group (DM-NRG)[30] in combination with the renown Z-trick method[31], which improves spectral resolution at high energies.

III. RESULTS

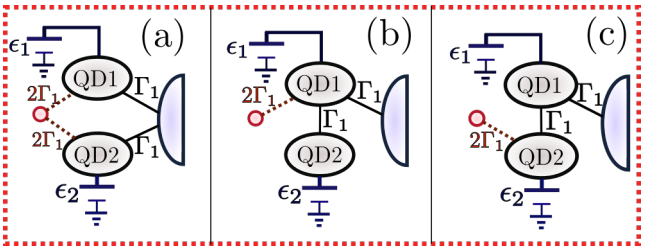

FIG. 2: Cases of study: (a) Symmetric coupling of the DQD to the lead and the MZM. No inter-dot coupling. (b)&(c) Indirect coupling of the second QD through the first dot. The Majorana is coupled to the (b) first dot or to the (c) second dot.

We call MZM manipulation to the "movements" attributed to the Majorana signature under the tunning of the dot gate voltages (ϵ_1, ϵ_2). This manipulation process is performed in three different set ups that are presented in Fig.2 with definite values of Γ_2, t_dots, t_1 and t_2. In configuration (a), we coupled the QD symmetrically to the lead and the Majorana mode. With this setup we expect to break the localization of the MZM which should split and tunnel into both dots. In setups (b) and (c) we coupled the second dot indirectly through the first dot. Hence, quantum interference should split the zero mode in two states. Our objective is to observe what occurs with the Majorana signature in this situation. There are two options to connect the MZM in this situation. Attached it directly through the first dot (b) or indirectly

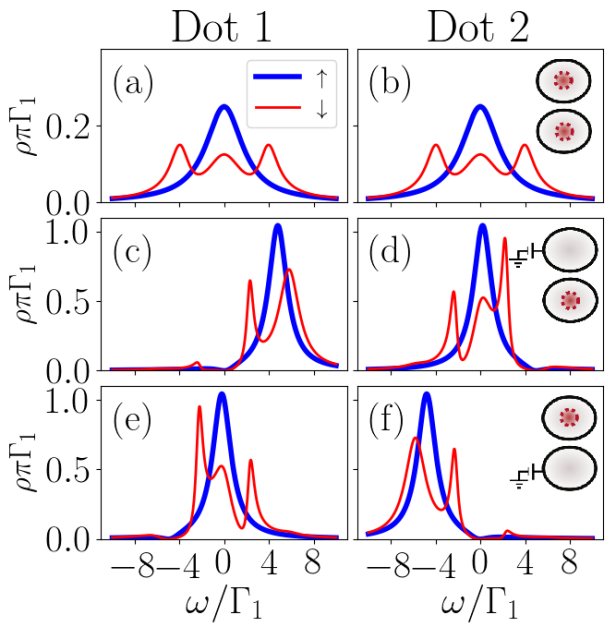

FIG. 3: Non-interacting DOS in the symmetric coupling setup (Fig.2(a)). Bold blue lines: Spin-↑ DOS. Thin red lines: Spin-↓ DOS.

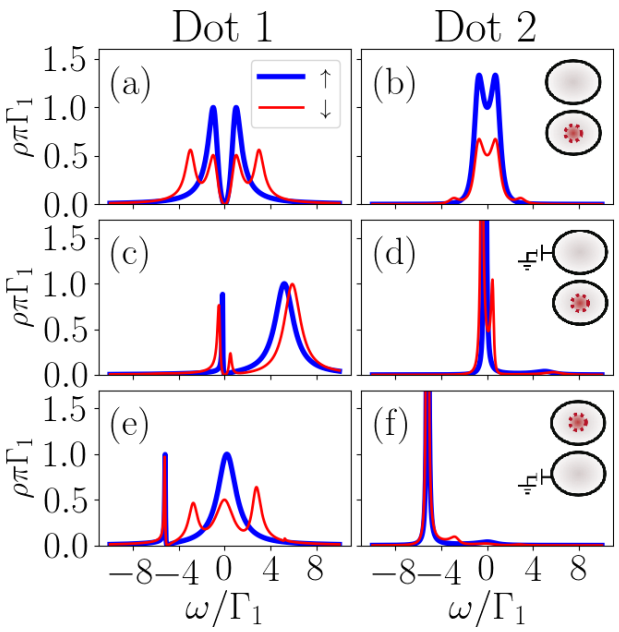

FIG. 4: Non-interacting DOS of the setup in Fig.2(b) . Bold blue lines: Spin-↑ DOS. Thin red lines: Spin-↓ DOS.

through the second dot (c).

A. MZM manipulation in non-interacting quantum dots

The non-interacting results for setups (a),(b) and (c) of FIG.2 are shown at figures FIG.3, FIG.4 and FIG.5 respectively. Each figure depicts the DOS of dot 1(left) and dot 2(right). The gate voltage is initially 0 in both dots at the first row. In the second row the gate voltage is turned on to $\epsilon_1 = 5\Gamma_1$ in the first dot and remains at $\epsilon_2 = 0$ in the second dot. In the third row the first dot's voltage is off $\epsilon_1 = 0$ and we switch on the second dot with a negative voltage of $\epsilon_2 = -5\Gamma_1$. The insets at each row shows which dots exhibit Majorana signatures, depicted by a red dashed circle inside the dot. These images will continuously change under the tuning of gate voltages which represents the manipulation of the Majorana signature.

In FIG.3 we observe the results for the symmetric coupling setup FIG.2(a). In the particle hole symmetric case (first row) the DOS is equal in both dots. Note that that the spin-↓ (Thin red line) DOS is the half of the spin-↑ (Bold blue line) DOS at the Fermi energy ($\rho_\downarrow(0) = \frac{1}{2}\rho_\uparrow(0)$). This type II Majorana signature is similar to the one observed when a single dot is coupled to a Majorana mode.[15] We may conclude that the Majorana in tunneling inside both dots breaking the localization of the MZM. If a positive or negative gate voltage is induced in one of the dots, as shown in the second and third row of Figure 3(c)-(f), the Majorana zero mode vanishes from that dot. Meanwhile the density of states in the other dot increases while preserving the Majorana signature. This means that the MZM is actually being induced to "leave" this dots and leak into the other dot by the gate voltage activation. This first example of MZM manipulation.

Another example of MZM manipulation occurs when the second dot is not directly connected to the lead. In this case, the inter-dot tunneling generates quantum interference which finally destroys the central peak as observe in FIG.4(a) at the spin-↑ DOS . The spin-↓ channel at FIG.4(a), which is coupled to the MZM, does not exhibit the characteristic Fermi peak either. Instead, the one half Majorana signature at the Fermi energy ($\rho_\downarrow(0) = \frac{1}{2}\rho_\uparrow(0)$) appears clearly inside the second dot FIG.4(b). This situation prevails when the first dot's gate voltage is turned on FIG.4(c)&(d). While the first dot does not seem to exhibit any type of Majorana signature, the second dot's spin-↓ DOS exhibits a robust zero-mode of height $\frac{0.5}{\pi\Gamma}$. The results are more exciting when the second dot's gate voltage is turned on in FIG.4(e)&(f). These figures clearly show how the MZM, previously localized at the second dot, is induced to leave this dot and returned onto the first dot. Moreover, the DOS of spin-↑ and spin-↓ channels are very similar to the spectral densities observed at FIG.3(d)(e), which means that the previous interference pattern has disappeared due to the presence of this gate voltage.

The results of the third configuration FIG.2(c) appear in FIG.5. Contrary to what was observed in the previous

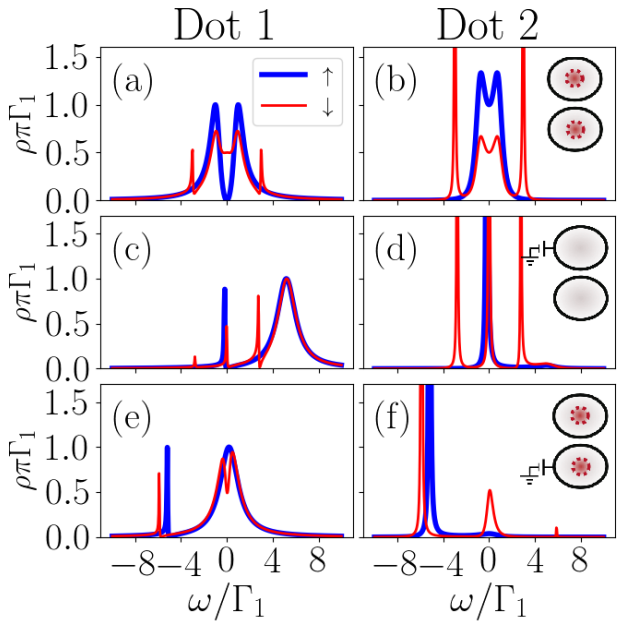

FIG. 5: Non-interacting DOS of the set up in Fig.2(c) . Bold blue lines: Spin-↑ DOS. Thin red lines: Spin-↓ DOS..

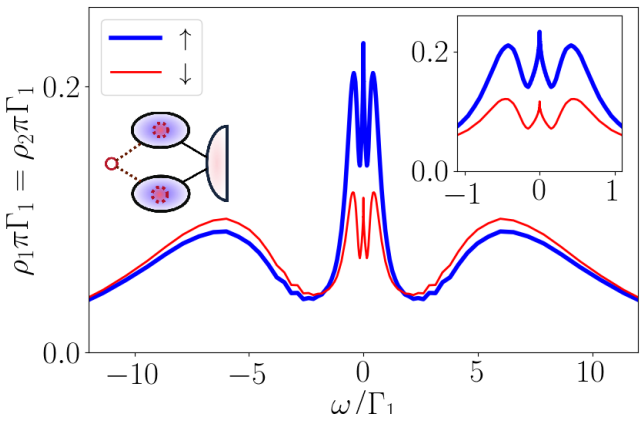

FIG. 6: Density of states of both dots in the symmetric coupling without gate voltages between the Majorana and the interacting DQD. Bold blue lines: Spin-↑ DOS. Thin red lines: Spin-↓ DOS.

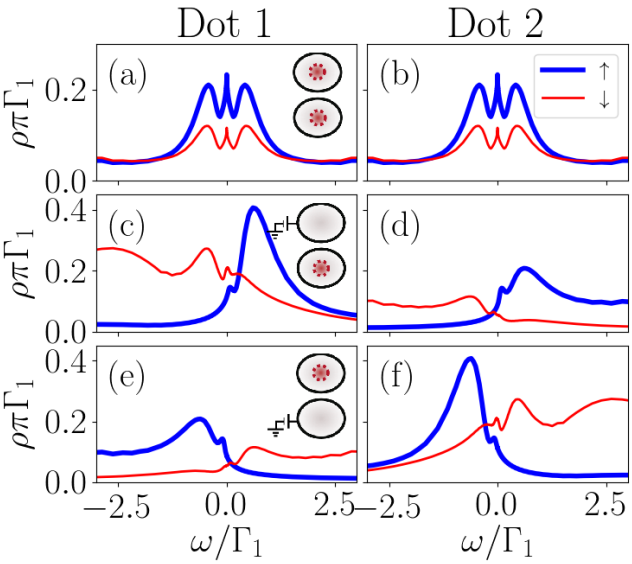

FIG. 7: Interacting DOS in the symmetric coupling setup (Fig.2. Bold blue lines: Spin-↑ DOS. Thin red lines: Spin-↓ DOS.

case, this time the Majorana signature is not destroyed by the interference but instead, the $\frac{0.5}{\pi\Gamma}$-height MZM emerges indirectly in the first dot. This is a perfect way to separate the Majorana's spin-↓ DOS from the central spin-↑ zero-mode which is still destroyed by the interference. In addition, the second dot still exhibits a type I Majorana signature as observed in FIG.5(b). In the second row we observe that turning on the gate voltage in dot 1 destroys the Majorana signature in both dots FIG.5(c)(d). On the other hand, if the second dot's voltage is switched both dots will preserve their Majorana signature (QD1:type I, QD2: type II), while the spin-↑ quantum interference vanishes in the first dot.

B. MZM manipulation in interacting dots

Now we consider a Coulomb repulsion energy of $U = 17\Gamma_1$ in both dots. The factor $\frac{U_i}{2}(\sum_\sigma \hat{n}_{i\sigma} - 1)^2$ in (2) favors states with an odd number of electrons (and holes). In addition, particle-hole equilibrium is now achieved when $\left(\epsilon_{di} + \frac{U_i}{2}\right)\hat{n}_{i\sigma}$. Any induced gate voltage must be considered as a shifting from this equilibrium point. FIG6 shows the DOS at both QDs for the symmetric coupling configuration 2. The two peaks appearing at around $8.6\Gamma_1 = \frac{U_i}{2}$ represent the two energy levels spaced by the Coulomb repulsion factor U. The central spin-↑ peak is a consequence of the Kondo effect,[27,32] while the two satellite peaks observed in the inset are the result of the RKKY indirect interaction between both dots.[21–23] Moreover, the system presents a Majorana signature characterized by half spin-↓ DOS at the Fermi energy ($\rho_\downarrow(0) = \frac{1}{2}\rho_\uparrow(0)$) . Note, that in this case the Majorana signature coexists with the Kondo effect in the DQD as already predicted by Ruiz-Tijerina *et al.* for a single dot.[18]

In this part project we are interested in the physics at low energy scales $\omega \sim \Gamma_1$ close to the Kondo and MZM temperature. At this scale we can observe simlar res results with the non-interacting results. For instance, FIG.7 shows the NRG results for the symmetric setup in FIG.2(a). In agreement with the non-interacting results, both dots have type I Majorana signatures. These sig-

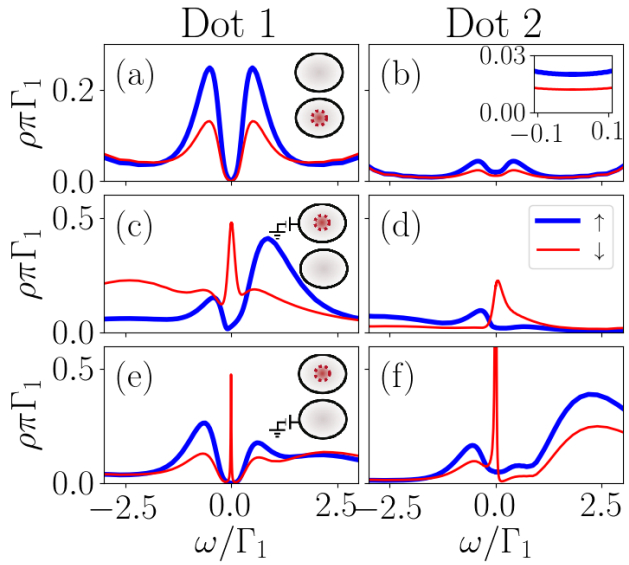

FIG. 8: Interacting DOS of the setup in Fig.2(b) . Bold blue lines: Spin-↑ DOS. Thin red lines: Spin-↓ DOS.

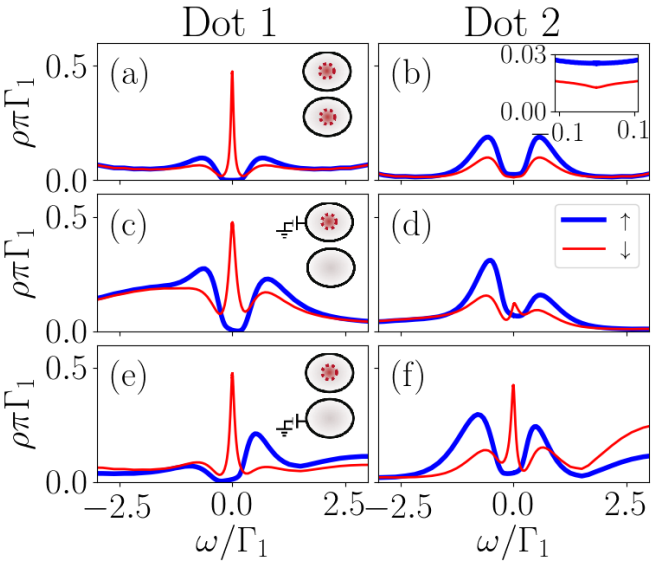

FIG. 9: Interacting DOS of the set up in Fig.2(c) . Bold blue lines: Spin-↑ DOS. Thin red lines: Spin-↓ DOS.

natures can be manipulated by tuning one of the dot's gate voltage to induce the MZM to leak into the other dot. The DOS at figures FIG.7(d)(e) shows a type I Majorana signature with $\rho_\downarrow(0) \approx \frac{1}{2}\rho_\uparrow(0)$). We observed that this Majorana signature is stable for adjustments of energies bellow the $6\Gamma_1$. At larger gate voltages the signal is destroyed.

In the second setup FIG.2(b), the NRG results in FIG.8 exhibit Majorana signatures similar to the non-interacting case. In the first row, the Majorana signature is destroyed by quantum interference while the second dot presents a type I Majorana signature as can be observed in the inset of the second dot. The first difference occurs when the gate voltage is switch on the first dot. This time the Majorana mode jumps onto the first dot which presents a type I Majorana signature . If the voltages is switched on the second dot, a type 2 Majorana signature appears a very low energies in dot 1.

Finally, FIG.9 show the NRG results for the last configuration FIG.2(c). Surprisingly, the indirectly attached MZM exhibits a robust type II Majorana signature in the first dot over a destroyed Kondo peak. This signature is stable under the gate voltage tuning. In addition, only the first in the particle hole symmetric case the second dot presents a type II Majorana signature (Inset FIG.9(b)). The difference between this model and the other that leads to a stable signature in one of the dots occurs because the QD's in the (c) model are connected in series. Therefore, the Majorana mode will always prevail in the dot that is attached to the leads besides the application of gate voltages. This case is similar to the model of a single dot attached to a Majorana chain, where it is known that the Majorana signatures is not disturbed by the gate tuning.

IV. CONCLUDING REMARKS

Comparing the exact analytical solution in the non-interacting system and the NRG results for interacting quantum dots, we were able to characterized the displacements of the MZM inside the double quantum dot for the three setups in FIG.2. We observe a considerable agreement on the location of the Majorana signature between the interacting and non-interacting results:

FIG.2(a): In the symmetric coupling the MZM leaks inside both dots. For interacting dots, the Majorana signature will be distinguishable near the Kondo temperature. At this regime the system presents combined Kondo-Majorana physics . If the gate voltage of one dot is turned on the MZM is induced to tunnel only into the other dot.

FIG.2(b): In this system the spin-↑ zero mode at QD1 (The Kondo peak if the system is interacting) is destroyed by quantum interference with the second dot. This interference will also destroy the MZM in the first dot but a type I Majorana signature will still appear in the second dot. The Majorana mode can be induced to tunnel back into the first dot if a gate voltage is applied on the second dot. This signature is visible at very low energies (bellow $0.1\Gamma_1$) in interacting case.

FIG.2(c): An indirect type II Majorana signature is observed in the first dot. This signature is robust, specially in the interacting case, where it is present in all configurations.

ACKNOWLEDGMENTS

The authors thank Edson Vernek for enlightening discussions. L.G.G.V.D.S. acknowledges financial support by CNPq (grants No. 307107/2013-2 and 449148/2014-9), and FAPESP (grant No. 2016/18495-4).

[1] J. Alicea, Reports on Progress in Physics **75**, 076501 (2012).
[2] C. Beenakker, Annual Review of Condensed Matter Physics **4**, 113 (2013).
[3] A. Y. Kitaev, Physics-Uspekhi **44**, 131 (2001).
[4] A. Y. Kitaev, Annals of Physics **303**, 2 (2003), arXiv: quant-ph/9707021.
[5] V. Mourik, K. Zuo, S. M. Frolov, S. R. Plissard, E. P. a. M. Bakkers, and L. P. Kouwenhoven, Science **336**, 1003 (2012).
[6] A. Das, Y. Ronen, Y. Most, Y. Oreg, M. Heiblum, and H. Shtrikman, Nature Physics **8**, 887 (2012).
[7] M. T. Deng, C. L. Yu, G. Y. Huang, M. Larsson, P. Caroff, and H. Q. Xu, Nano Letters **12**, 6414 (2012).
[8] S. Nadj-Perge, I. K. Drozdov, J. Li, H. Chen, S. Jeon, J. Seo, A. H. MacDonald, B. A. Bernevig, and A. Yazdani, Science **346**, 602 (2014).
[9] M. T. Deng, S. Vaitiekenas, E. B. Hansen, J. Danon, M. Leijnse, K. Flensberg, J. Nygard, P. Krogstrup, and C. M. Marcus, Science **354**, 1557 (2016).
[10] H. Zhang, C.-X. Liu, S. Gazibegovic, D. Xu, J. A. Logan, G. Wang, N. van Loo, J. D. S. Bommer, M. W. A. de Moor, D. Car, R. L. M. Op het Veld, P. J. van Veldhoven, S. Koelling, M. A. Verheijen, M. Pendharkar, D. J. Pennachio, B. Shojaei, J. S. Lee, C. J. Palmstrøm, E. P. A. M. Bakkers, S. D. Sarma, and L. P. Kouwenhoven, Nature **556**, 74 (2018).
[11] E. J. H. Lee, X. Jiang, R. Aguado, G. Katsaros, C. M. Lieber, and S. De Franceschi, Physical Review Letters **109**, 186802 (2012).
[12] D. Aasen, M. Hell, R. V. Mishmash, A. Higginbotham, J. Danon, M. Leijnse, T. S. Jespersen, J. A. Folk, C. M. Marcus, K. Flensberg, and J. Alicea, Physical Review X **6**, 031016 (2016).
[13] S. D. Sarma, M. Freedman, and C. Nayak, npj Quantum Information **1**, 15001 (2015).
[14] B. v. Heck, A. R. Akhmerov, F. Hassler, M. Burrello, and C. W. J. Beenakker, New Journal of Physics **14**, 035019 (2012).
[15] D. E. Liu and H. U. Baranger, Physical Review B **84** (2011), 10.1103/PhysRevB.84.201308, arXiv: 1107.4338.
[16] E. Vernek, P. H. Penteado, A. C. Seridonio, and J. C. Egues, Physical Review B **89**, 165314 (2014).
[17] M. Lee, J. S. Lim, and R. Lopez, Physical Review B **87**, 241402 (2013).
[18] D. A. Ruiz-Tijerina, E. Vernek, L. G. G. V. Dias da Silva, and J. C. Egues, Physical Review B **91**, 115435 (2015).
[19] M. Barkeshli and J. D. Sau, arXiv:1509.07135 [cond-mat, physics:quant-ph] (2015), arXiv: 1509.07135.
[20] T. Karzig, C. Knapp, R. M. Lutchyn, P. Bonderson, M. B. Hastings, C. Nayak, J. Alicea, K. Flensberg, S. Plugge, Y. Oreg, C. M. Marcus, and M. H. Freedman, Physical Review B **95**, 235305 (2017).
[21] M. A. Ruderman and C. Kittel, Physical Review **96**, 99 (1954).
[22] T. Kasuya, Progress of Theoretical Physics **16**, 45 (1956).
[23] K. Yosida, Physical Review **106**, 893 (1957).
[24] L. G. G. V. Dias da Silva, N. Sandler, K. Ingersent, and S. E. Ulloa, Physica E: Low-dimensional Systems and Nanostructures **40**, 1002 (2008).
[25] D. N. Zubarev, Soviet Physics Uspekhi **3**, 320 (1960).
[26] D. A. Spielman, *Algorithms, Graph Theory, and Linear Equations in Laplacian Matrices*, Proceedings of the International Congress of Mathematicians (2010).
[27] K. G. Wilson, Reviews of Modern Physics **47**, 773 (1975).
[28] M. Sindel, *Numerical Renormalization Group studies of Quantum Impurity Models in the Strong Coupling Limit*, Text.PhDThesis, Ludwig-Maximilians-Universität München (2005).
[29] R. Bulla, T. A. Costi, and T. Pruschke, Reviews of Modern Physics **80**, 395 (2008).
[30] W. Hofstetter, Physical Review Letters **85**, 1508 (2000).
[31] W. C. Oliveira and L. N. Oliveira, Physical Review B **49**, 11986 (1994).
[32] A. C. Hewson, *The Kondo Problem to Heavy Fermions* (Cambridge University Press, 1997) google-Books-ID: fPzgHneNFDAC.

Appendix A: Computation of the Green Function

In Zubarev's fermionic ballistic transport approach[25] the green function associated to two operators $A(t)$, $B(t)$ is defined as that Fourier transform of the time-ordered anti-commutator of A and B

$$G_{A,B}(\omega) = \mathcal{F}\left\{\mathcal{T}\left[\{A(t), B(t')\}\right]\right\}(\omega)\,. \tag{A1}$$

The Fourier transform of Schrodinger evolution leads to the the transport equations

$$\omega G_{A,B}(\omega) = \delta_{A^\dagger,B} + G_{[A,H],B}(\omega). \tag{A2}$$

Applying this expression to Hamiltonian (1) replacing A and B by the creation and annihilation operators $d\dagger_i, f^\dagger, d_i, f, c_k, c\dagger_k$ we obtain a linear transport system. To simplify the complexity of the equations we fix $B = d^\dagger_{1\downarrow}$. In addition note that if we replace A by $f_\downarrow$ and $f^\dagger_\downarrow$ A2 becomes

$$(\omega - \epsilon_M)\, G_{f_\downarrow, d^\dagger_{1\downarrow}}(\omega) = \frac{t}{\sqrt{2}}\left(G_{d_{1\downarrow}, d^\dagger_{1\downarrow}}(\omega) - G_{d^\dagger_{1\downarrow}, d^\dagger_{1\downarrow}}(\omega)\right) \tag{A3}$$

$$(\omega + \epsilon_M)\, G_{f^\dagger_\downarrow, d^\dagger_{1\downarrow}}(\omega) = \frac{t}{\sqrt{2}}\left(G_{d_{1\downarrow}, d^\dagger_{1\downarrow}}(\omega) - G_{d^\dagger_{1\downarrow}, d^\dagger_{1\downarrow}}(\omega)\right). \tag{A4}$$

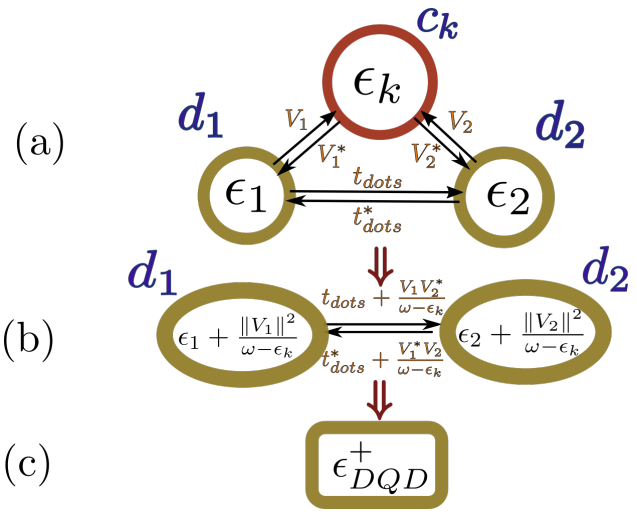

FIG. 10

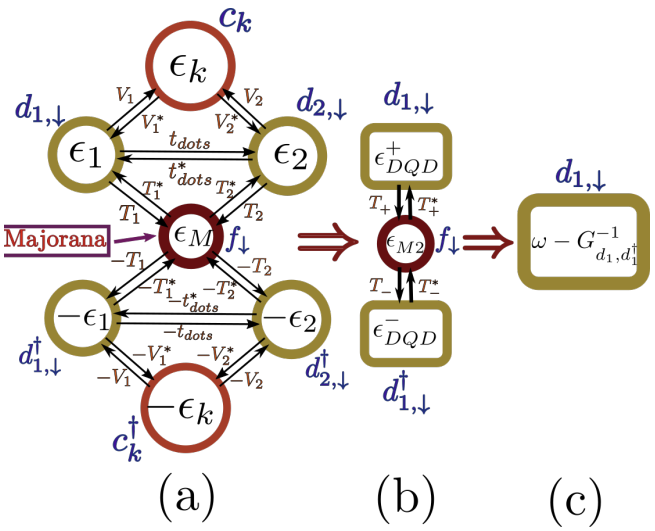

FIG. 11: Transport flow in a DQD Majorana system.

This allows us to take $G_{f^\dagger_\downarrow,d^\dagger_{1\downarrow}}(\omega) = \frac{\omega+\epsilon}{\omega-\epsilon}G_{f^\dagger_\downarrow,d^\dagger_{1\downarrow}}(\omega)$. Hence, we can eliminate $G_{f^\dagger_\downarrow,d^\dagger_{1\downarrow}}(\omega)$ from the equations even before we start Gauss-Jordan process.

Writing the other equations we obtain the linear system of the form

$$\mathcal{T}\vec{G}_{d_1^\dagger} = \hat{e_1}, \tag{A5}$$

where $\mathcal{T}$ is the transport matrix

$$\begin{bmatrix} \omega-\epsilon_1 & -V_1^* & -t_{dots} & \frac{-t_1}{\sqrt{2}} & 0 & 0 & 0 \\ -V_1 & \omega-\epsilon_k & -V_2 & 0 & 0 & 0 & 0 \\ -t_{dots}^* & -V_2^* & \omega-\epsilon_2 & \frac{-t_2}{\sqrt{2}} & 0 & 0 & 0 \\ \frac{-\sqrt{2}t_1^*}{\omega+\epsilon_M} & 0 & \frac{-\sqrt{2}t_2^*}{\omega+\epsilon_M} & \omega-\epsilon_M & \frac{\sqrt{2}t_2^*}{\omega+\epsilon_M} & 0 & \frac{\sqrt{2}t_1^*}{\omega+\epsilon_M} \\ 0 & 0 & 0 & \frac{t_2}{\sqrt{2}} & \omega+\epsilon_2 & V_2^* & t_{dots}^* \\ 0 & 0 & 0 & 0 & V_2 & \omega+\epsilon_k & V_1 \\ 0 & 0 & 0 & \frac{t_1}{\sqrt{2}} & t_{dots} & V_1^* & \omega+\epsilon_1 \end{bmatrix}, \tag{A6}$$

$\vec{G}_{d_1^\dagger}$ is the column vector

$$[G_{d_{1\downarrow},d^\dagger_{1\downarrow}}(\omega), G_{c_{k\downarrow},d^\dagger_{1\downarrow}}(\omega), G_{d_{2\downarrow},d^\dagger_{1\downarrow}}(\omega), G_{f_\downarrow,d^\dagger_{1\downarrow}}(\omega), G_{d^\dagger_{2\downarrow},d^\dagger_{1\downarrow}}(\omega), G_{c^\dagger_{k\downarrow},d^\dagger_{1\downarrow}}(\omega), G_{d^\dagger_{1\downarrow},d^\dagger_{1\downarrow}}(\omega)]^T$$

and $\hat{e_1}$ is the vector with entries $\hat{e}_{1_n} = \delta_{1n}$.

The graph associated to this matrix is the one in FIG.11. The energies inside each vertex are given by subtracting the corresponding diagonal term from ω . The couplings are just the negative of the off-diagonal terms.

1. The double quantum dot

To explain the process of Gaussian elimination we will obtain the green function for the case without Majorana fermion ($t_1 = t_2 = 0$). The transport matrix for this system is

$$\begin{bmatrix} \omega-\epsilon_1 & -V_1 & -t_{dots} \\ -V_1^* & \omega-\epsilon_k & -V_2 \\ -t_{dots}^* & -V_2^* & \omega-\epsilon_2 \end{bmatrix}. \tag{A7}$$

The graph associated to this matrix can be observed in FIG10.a). To eliminate the vertex c_k we just need to subtract from (A7) the rank-1 matrix that cancels the row and the column corresponding to c_k. This matrix is

$$\begin{bmatrix} \frac{V_1^*V_1}{\omega-\epsilon_k} & -V_1^* & \frac{V_2V_1^*}{\omega-\epsilon_k} \\ -V_1 & \omega-\epsilon_k & -V_2 \\ \frac{V_2^*V_1}{\omega-\epsilon_k} & -V_2^* & \frac{V_2^*V_2}{\omega-\epsilon_k} \end{bmatrix}. \tag{A8}$$

The result of (A7) - (A8) is

$$\begin{bmatrix} \omega-\epsilon_1-\frac{V_1^*V_1}{\omega-\epsilon_k} & 0 & -t_{dots}-\frac{V_2V_1^*}{\omega-\epsilon_k} \\ 0 & 0 & 0 \\ -t_{dots}^*-\frac{V_2^*V_1}{\omega-\epsilon_k} & 0 & \omega-\epsilon_2-\frac{V_2V_1^*}{\omega-\epsilon_k} \end{bmatrix} \tag{A9}$$

which is depicted by the graphs in FIG.10.b). The next step is to pop-out the vertex d_2 following the same procedure. At the end, the energy inside the vertex d_1 will be

$$\epsilon^+_{DQD} = \epsilon_1 + \sum_{\mathbf{k}}\frac{V_1V_1^*}{\omega-\epsilon_{\mathbf{k}}} + \frac{\left\|t_{dots}+\sum_{\mathbf{k}}\frac{V_1V_2^*}{\omega-\epsilon_{\mathbf{k}}}\right\|^2}{\omega-\epsilon_2-\sum_{\mathbf{k}}\frac{V_2V_2^*}{\omega-\epsilon_{\mathbf{k}}}} \tag{A10}$$

and the green function of $G_{d_1d_1^\dagger}(\omega)$ in a DQD will be given by $\frac{1}{\omega-\epsilon_{DQD}}$ (see FIG.10.c)).

2. Solution of the transport equations

The previous procedure can be generalized into the following algorithm:

1. Computing the transport equations with the second term fixed in the creation operator of the dot.
2. Setting up the graph associated to the transport system.
3. Popping out the vertexes of the graph. Each popping process carries the following steps.
   (a) Computing the extra-terms in the energies and couplings based on the walks passing through the popped vertex.
   (b) Eliminating this vertex from the graph.
   (c) Iterating till there is only one vertex.
4. The energy in the remaining vertex d is $\epsilon_d = \frac{1}{\omega - G_{d,d\dagger}(\omega)}$.

Following these steps it is possible to solve the general case. We start with the graph in FIG.11 and we pop out the vertexes $c_k, c_k^\dagger, d_{2,\downarrow}$ and $d_{2,\downarrow}^\dagger$ in that order. The energies associated to $d_{1,\downarrow}$ and $d_{1,\downarrow}^\dagger$ will be similar to (A10) giving

$$\epsilon_{DQD}^{\pm} = \pm\epsilon_1 + \sum_{\mathbf{k}} \frac{V_1 V_1^*}{\omega - \epsilon_{\mathbf{k}}} + \frac{\left\| \pm t_{dots} + \sum_{\mathbf{k}} \frac{V_1 V_2^*}{\omega - \epsilon_{\mathbf{k}}} \right\|^2}{\omega \pm \epsilon_2 - \sum_{\mathbf{k}} \frac{V_2 V_2^*}{\omega - \epsilon_{\mathbf{k}}}}. \tag{A11}$$

There is also a correction in the couplings between the Majorana mode and $d_{1,\downarrow}$, $d_{1,\downarrow}^\dagger$ given by

$$T_{\pm} = \pm t_1 \pm t_2 \frac{\left(\pm t_{dots} + \sum_{\mathbf{k}} \frac{V_1 V_2^*}{\omega - \epsilon_{\mathbf{k}}} \right)}{\omega \pm \epsilon_2 \pm \sum_{\mathbf{k}} \frac{V_2 V_2^*}{\omega - \epsilon_{\mathbf{k}}}}. \tag{A12}$$

Finally since the Majorana is in contact with dot 2, there is an extra-term appearing in the Majorana energy given by

$$\epsilon_{M2} = \omega - \epsilon_M - \frac{\frac{\omega}{\omega + \epsilon_M} \|t_2\|^2}{\omega - \epsilon_2 - \sum_{\mathbf{k}} \frac{V_2 V_2^*}{\omega - \epsilon_{\mathbf{k}}}} - \frac{\frac{\omega}{\omega + \epsilon_M} \|t_2\|^2}{\omega + \epsilon_2 - \sum_{\mathbf{k}} \frac{V_2 V_2^*}{\omega + \epsilon_{\mathbf{k}}}}. \tag{A13}$$

With all the terms of the graph in FIG.11.b) computed, it only remains to pop out vertexes $d_1^\dagger$ and $f_\downarrow$ in that order to obtain the result in equation (11).

$$G_{d_{1\downarrow}, d_{1\downarrow}^\dagger}(\omega) = \frac{1}{\omega - \epsilon_{DQD}^{+} - \frac{\|T_+\|^2}{\omega - \epsilon_{M2} - \frac{\|T_-\|^2}{\epsilon_{DQD}^{-}}}}. \tag{A14}$$

From this analytical expression we can compute rapidly dynamical quantities such as the density of states in the non-interacting regime. Despite the difference this became a useful idea to predict interesting parameters for NRG simulation. Since the NRG code code takes about an hour to simulate each set of parameters in the Majorana-DQD mode, and even more if additional implementations are necessary, A14 became an important tool to improve our results.